AGU PUBLICATIONS

JGR

Journal of Geophysical Research: Solid Earth

RESEARCH ARTICLE

10.1002/2014JB011498

Key Points:
- Strain accumulation in the New Madrid region is within error of zero
- Strain accumulation in the Wabash Valley region is within error of zero
- CEUS behaves as a rigid plate, to within the level of noise

Supporting Information:
- Readme
- Figure S1
- Figure S2
- Figure S3
- Figure S4
- Table S1

Correspondence to:
T. J. Craig,
craig@geologie.ens.fr

Citation:
Craig, T. J., and E. Calais (2014), Strain accumulation in the New Madrid and Wabash Valley seismic zones from 14 years of continuous GPS observation, *J. Geophys. Res. Solid Earth*, *119*, doi:10.1002/2014JB011498.

Received 29 JUL 2014
Accepted 27 OCT 2014
Accepted article online 30 OCT 2014

Strain accumulation in the New Madrid and Wabash Valley seismic zones from 14 years of continuous GPS observation

Timothy J. Craig[1] and Eric Calais[1]

[1] Ecole Normale Supérieure, Department of Geosciences, UMR CNRS 8538, Paris, France

Abstract The mechanical behavior—and hence earthquake potential—of faults in continental interiors is an issue of critical importance for the resultant seismic hazard, but no consensus has yet been reached on this controversial topic. The debate has focused on the central and eastern United States, in particular, the New Madrid Seismic Zone, struck by four magnitude 7 or greater earthquakes in 1811–1812, and to a lesser extent the Wabash Valley Seismic Zone just to the north. A key aspect of this issue is the rate at which strain is currently accruing on those plate interior faults, a quantity that remains debated. Here we address this issue with an analysis of up to 14.6 years of continuous GPS data from a network of 200 sites in the central United States centered on the New Madrid and Wabash Valley seismic zones. We find that the high-quality sites in these regions show motions that are consistently within the 95% confidence limit of zero deformation. These results place an upper bound on strain accrual on faults of 0.2 mm/yr and 0.6 mm/yr in the New Madrid and Wabash Valley Seismic Zones, respectively. For the New Madrid region, where a paleoseismic record is available for the past ~5000 years, we argue that strain accrual—if any—does not permit the 500–900 year repeat time of paleo-earthquakes observed in the Upper Mississippi Embayment. These results, together with increasing evidence for temporal clustering and spatial migration of earthquake sequences in continental interiors, indicate that either tectonic loading rates or fault properties vary with time in the New Madrid Seismic Zone and possibly plate wide.

1. Introduction

Geodetic studies at plate boundaries have long shown that plate motions are accommodated by elastic deformation of the Earth's crust that accumulates at steady rates near active faults. This elastic strain is released episodically by sudden fault slip during large earthquakes so that, over a few hundred years, balance is achieved between the rates at which strain accumulates and is released. Whether this steady state model—which forms the basis for probabilistic seismic hazard calculations—applies to continental plate interiors, where large earthquakes are much less frequent than at plate boundaries, is an unresolved question.

The New Madrid Seismic Zone (NMSZ) (Figure 1) has been the focal point for this issue because it is a type example for large intracontinental earthquakes. Four magnitude 7 or greater earthquakes struck the area in 1811–1812 [*Johnston*, 1996; *Hough et al.*, 2000], making earthquake hazard assessment a high priority in this heavily populated area of the North American midcontinent. The neighboring Wabash Valley Seismic Zone (WVSZ) also shows elevated seismic activity [*Nuttli and Brill*, 1981], with one $M \geq 7$ paleo-earthquake dated at about 6 Ka [*Obermeier*, 1998]. Whether the WVSZ is independent from the NMSZ or might be the next focus in a migratory sequence of intraplate earthquake clusters [e.g., *Galgana and Hamburger*, 2010] is an important question for regional seismic hazard and for understanding earthquake processes in plate interiors.

It is classically assumed that faults in stable continental interiors behave like those at plate boundaries, accumulating strain at a rate consistent with the seismic record so that large earthquakes occur at similar locations and quasi-regular time intervals. There is however evidence from the paleo-earthquake record that faults in such a setting may operate differently, with very long periods of seismic quiescence separated by short periods of clustered activity, so that the loci of large earthquakes migrate over time among fault systems within a continent [*Crone et al.*, 2003]. In this hypothesis, currently active seismic zones such as the New Madrid region may represent aftershocks of large historical earthquakes rather than evidence for current

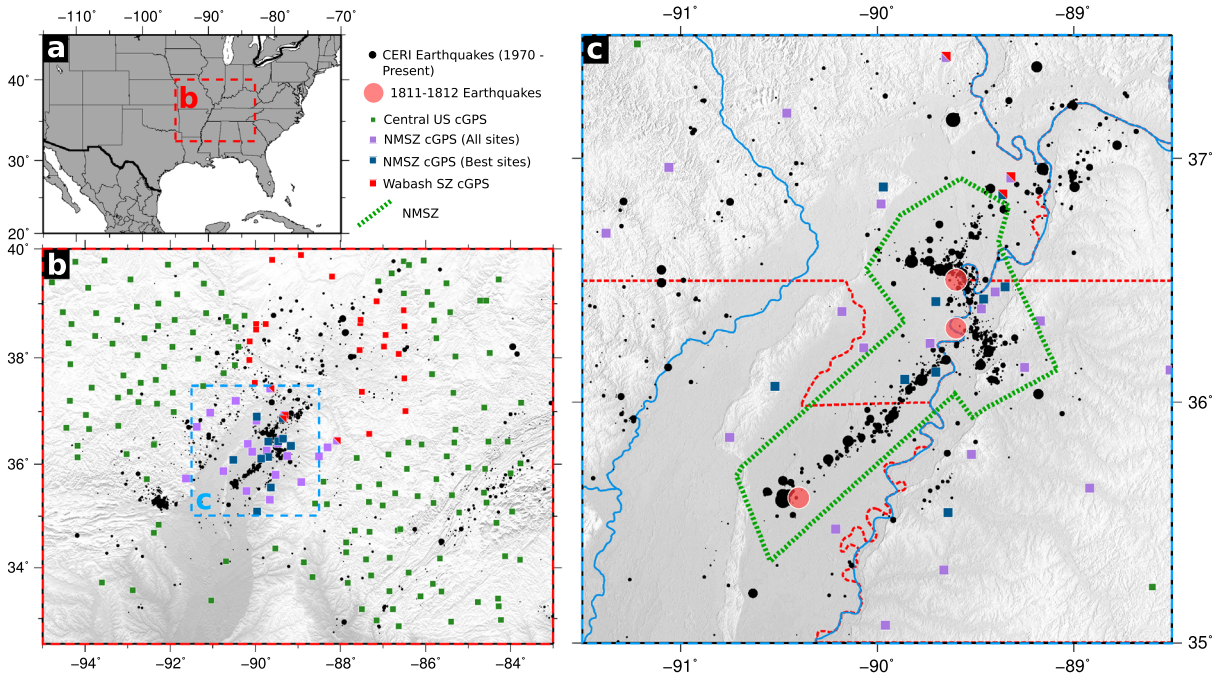

Figure 1. (a) Location map for eastern North America. (b) Continuous GPS sites included in this study. Those identified as "NMSZ" or "Wabash" are the specific sites focused on when considering the strain accumulation in these areas. Sites identified as "best" are the 11 sites with the longest and cleanest time series around the NMSZ. Seismicity is taken from the CERI earthquake catalog for the Central and Eastern United States (http://www.memphis.edu/ceri). (c) The New Madrid Seismic Zone (dashed green contour). Red circles represent the 1811–1812 earthquake sequence, taken from the USGS Historical Earthquakes Catalogue.

strain accrual [*Stein and Liu*, 2009]. Geodetic results showing strain accrual at rates indistinguishable from zero in the NMSZ support this view [*Calais et al.*, 2006; *Calais and Stein*, 2009]. These geodetic results are however challenged by alternate studies arguing that strain in the NMSZ is significant [*Smalley et al.*, 2005; *Frankel et al.*, 2012]. If so, current seismicity in the NMSZ may be the manifestation of present-day strain accrual on the New Madrid faults [*Page and Hough*, 2014]. This strain accrual—even at slow rates—should become measurable as geodetic networks improve and observational time series duration increase.

Assessing current tectonic activity with geodetic instrumentation in stable continental interiors is a challenge because the very low expected strain rates are close to the measurement precision. Large-scale GPS measurements in North America and Europe show long wavelength horizontal (and vertical) deformation caused by Glacial Isostatic Adjustment (GIA) [*Nocquet et al.*, 2005; *Calais et al.*, 2006; *Sella et al.*, 2007], but conclusive evidence for strain accumulation at regional scale on specific fault zones remains elusive. A key criterion for identifying such tectonic deformation is a spatially coherent pattern of velocities, consistent over several neighboring geodetic sites. Meaningful statistical sampling therefore requires a dense network of GPS stations, which is now beginning to emerge in the Central Eastern U.S. (CEUS) (Figure 1). The recent increase in the number of continuously recording GPS stations in this region has led to a significant increase in the density of sites for which both accurate velocities and an estimate of the time-dependent noise (necessary for reliable quantification of the uncertainties) can be obtained. Here, we analyze data from 200 continuous GPS stations surrounding the New Madrid and Wabash Valley seismic zones of the CEUS, using data, when available, over a period extending from the start of 2000 through to mid-2014 to determine whether resolvable strain accumulation in the these regions can be detected geodetically with confidence.

2. Large Earthquakes and Current Strain Rates in the CEUS

Between December 1811 and February 1812, the region of southeastern Missouri and eastern Tennessee in the central United States (Figure 1c) was struck by a sequence of four significant earthquakes [*Fuller*, 1912; *Nuttli*, 1973]. Accurate magnitude estimates are difficult to obtain in this preinstrumental period, but macroseismic estimates for the largest earthquake indicate that it likely exceeded M_w 7.1 [*Hough and Page*, 2011]—although earlier studies proposed that it may have reached M_w 8 [*Johnston*, 1996]—with three

other earthquakes of similar magnitude occurring in a space of 4 months. These are some of the largest earthquakes known to have occurred in a continental intraplate setting.

Seismic activity in the region of the NMSZ continues to this day, although activity in the instrumental period rarely exceeds M_w 4. In terms of both historical and instrumental seismicity, the NMSZ represents a significant anomaly against the backdrop of the relatively seismically quiescent continental interior of North America, east of the Rocky Mountains (Figure 1). Paleoseismological indicators suggest that this region has experienced similar magnitude events over a time period extending back at least 3000 years [*Kelson et al.*, 1996; *Tuttle et al.*, 2005], with earthquakes occurring within the broad New Madrid region approximately every 500 years over that period [*Tuttle et al.*, 2002]. Geologically, the 1811–1812 sequence and the continuing seismicity are believed to represent reactivation and inversion of a subset of faults relict from the Cambrian Reelfoot Rift [*Van Arsdale*, 2009], with the majority of seismic activity limited to the upper crust, at depths of 5–15 km [*Dunn et al.*, 2010]. The degree to which this region represents a significant continuing seismic hazard has been the subject of much debate over the past decades. Space geodesy provides an obvious way of addressing this debate because of its ability to measure strain over regions of any size with a millimeter to submillimeter per year precision.

The search for intraplate deformation in the stable part of North America using space geodesy started with work by *Argus and Gordon* [1996] and *Dixon et al.* [1996], who used between nine and 20 sites in the plate interior to establish an upper bound of 2 mm/yr for residual motions across the CEUS. Other authors later found similar results [e.g., *Newman et al.*, 1999; *Kogan et al.*, 2000], although *Gan and Prescott* [2001] reported elevated strain in the south-central U.S. based on results at GPS station MEM2 in the Mississippi embayment, later discovered to be unstable. *Calais et al.* [2006] analyzed data from more than 300 continuous GPS sites in the North American plate interior and showed that their horizontal and vertical velocities could be fit within uncertainties by a rigid plate rotation combined with deformation from glacial isostatic adjustment (GIA). They reported that the impact of GIA on horizontal strain rates was negligible south of about 45°N, with a strain upper bound of 1.5×10^{-10} yr^{-1} corresponding to 0.5 mm/yr when integrated over the CEUS.

These plate-wide results however did not preclude that strain might accumulate at significant rates in regions where the density of GPS measurements was not sufficient to detect it, such as the New Madrid or Wabash Valley seismic zones. Indeed, an early study based on a comparison of GPS and terrestrial geodetic measurements reported 5–7 mm/yr of deformation across the southern part of the NMSZ [*Liu et al.*, 1992], consistent with a steady state fault system producing one M_w 8 earthquake every 500 to 1000 years [*Johnston*, 1996]. Similar measurements in the northern NMSZ were however inconclusive, with less than 3 mm/yr of motion across the fault system [*Snay et al.*, 1994]. Early episodic GPS measurements over the entire NMSZ found similar results, placing an upper limit of 2.5 mm/yr on deformation in the NMSZ [*Newman et al.*, 1999].

These results from episodic measurements were soon superseded by analyses of continuous GPS data. *Smalley et al.* [2005] reported strain rates in the NMSZ "comparable in magnitude to those across active plate boundaries," based on 1.4 mm/yr of shortening across a 10 km long baseline spanning the Reelfoot fault. This was later shown to result from an unexplained offset in the baseline between the two sites, while other data showed less than 0.7 mm/yr of deformation in the NMSZ as a whole [*Calais et al.*, 2005, 2006]. A subsequent reanalysis of the NMSZ continuous GPS data set led to an even smaller upper bound on site motions of 0.4 mm/yr [*Calais and Stein*, 2009], with all velocities in the NMSZ consistent with a rigid plate behavior within their 95% uncertainties. Most recently, *Frankel et al.* [2012] used relative site displacements to assess regional deformation in the NMSZ. They found significant displacement (0.37 ± 0.07 mm/yr) between GPS sites PTGV and STLE, which cross the inferred deep portion of the Reelfoot Fault (Figure 1c), and argued that this surface deformation was caused by aseismic slip at a rate of 4 mm/yr on the downdip part of the Reelfoot Fault between depths of 12 and 20 km. This, they argue, would produce sufficient loading for one M_w 7.3 earthquake every 500 years on the shallow portion of the fault. It remains, however, unclear whether these geodetic results reflect an actual tectonic process, the effect of local hydrology, monument instability, or the expected statistical behavior of a random distribution of many sites about a zero-displacement mean [*Boyd et al.*, 2013].

The cause of the 1811–1812 New Madrid earthquake sequence and the underlying physical process responsible for large earthquakes in plate interiors remain therefore enigmatic and controversial. Whether the present deformation reflects that observed from the geological records, how to interpret anomalous

displacements at isolated sites, whether there is present-day strain accrual, and whether there is any strain accrual in the surrounding regions remain questions on which there is little consensus. Recent increases in the number of continuously recording GPS receivers in the central United States have led to a large increase in the density of sites for which accurate velocities can be obtained, providing an opportunity to reassess these issues. Here we analyze both previously studied and newly available continuous GPS data in the Central and Eastern United States to determine if resolvable geodetic strain accumulation can be detected in this controversial region.

3. Data Processing

We select openly available continuous GPS sites for a region spanning 33° to 40° latitude by −95° to −83° longitude in the CEUS, centered on the NMSZ and also encompassing the Wabash Valley Seismic Zone (WVSZ). This yields a total of 200 continuous GPS sites with data duration ranging from 3 months to 14.6 years. We retrieve data from the UNAVCO (http://www.unavco.org/) and CORS (http://www.geodesy.noaa.gov/CORS/) archives, and process them using the GAMIT–GLOBK software package [*Herring et al.*, 2013, http://www-gpsg.mit.edu/~simon/gtgk]. We estimate daily positions along with seven daily tropospheric delay parameters per site, two parameters for horizontal tropospheric gradients, and satellite state vectors from doubly difference phase observations sampled at 30 s intervals. We apply automated phase ambiguity resolution at this stage, along with corrections for solid Earth tides, polar tides, and time variable ocean loading following the 2010 IERS conventions [*Petit and Luzum*, 2010]. We use final IGS orbits and Earth orientation parameters and apply a correction for antenna phase center variations using the latest IGS tables (*Schmid et al.* [2007], and subsequent updates).

Daily position time series for each site are visually inspected to identify any discontinuity or offsets, either documented and due to changes in instrumentation or sometimes undocumented. We exclude sections of some time series where they undergo apparent nonlinear deviation from the background trend due to instrument failure—this is the case, for example, for site RLAP between October 2005 and August 2009. We account for these discontinuities in the velocity solution by allowing for a single three-component offset while equating velocities before and after the offset.

Detrended three-component time series for these sites are shown in Figure 2 for a subset of sites covering the NMSZ. Although seasonal signals can clearly be seen in the position time series for a number of sites (e.g., site BLMM, Figure 2), we make no attempt to correct for this. These signals, at approximately annual and semiannual periods, are likely the result of unmodeled loading effects (hydrological and atmospheric) and average out over (at least) three cycles. Minimum influence on velocity estimates is seen for half-integer year duration time series [*Blewitt and Lavallée*, 2002]. Here we restrict our interpretation to time series with a minimum duration of 3.5 years. Monument quality is variable across the set of sites selected, which were designed for applications ranging from tectonic geodesy to structural surveying. This leads to noise characteristics that are highly site dependent with, in some cases, velocities influenced by local effects unrelated to the regional tectonics (a number of examples are discussed below). We therefore consider it important to base the interpretation on the local to regional coherence among neighboring sites rather than on individual velocities at single sites.

Once the position time series have been cleaned, we combine our regional loosely constrained daily solutions, along with the global daily solutions for the whole IGS network available from the Massachusetts Institute of Technology IGS Data Analysis Center, into weekly position solutions in order to improve signal resolution over the noise level and to optimally tie our solution to the International Terrestrial Reference Frame (ITRF) [*Altamimi et al.*, 2011]. We finally combine these weekly solutions into a single position/velocity solution using GLOBK [*Herring et al.*, 2013, http://www-gpsg.mit.edu/~simon/gtgk], which we tie to the ITRF by minimizing position and velocity deviations from a set of globally defined IGS reference sites common to our solution via a 12 parameter Helmert transform (scale and scale change are not estimated). We downweight the variance of the height coordinates by a factor of 10 in defining the reference frame because of the reduced precision of the vertical component in standard GPS solutions. We estimate time-correlated noise at each site using the First-Order Gauss-Markov Extrapolation (FOGMEx) algorithm of *Herring* [2003] (see also *Reilinger et al.* [2006]) in order to obtain realistic velocity uncertainties, which are discussed in more detail below. Table S1 in the supporting information presents velocity results for all sites in the Central U.S.

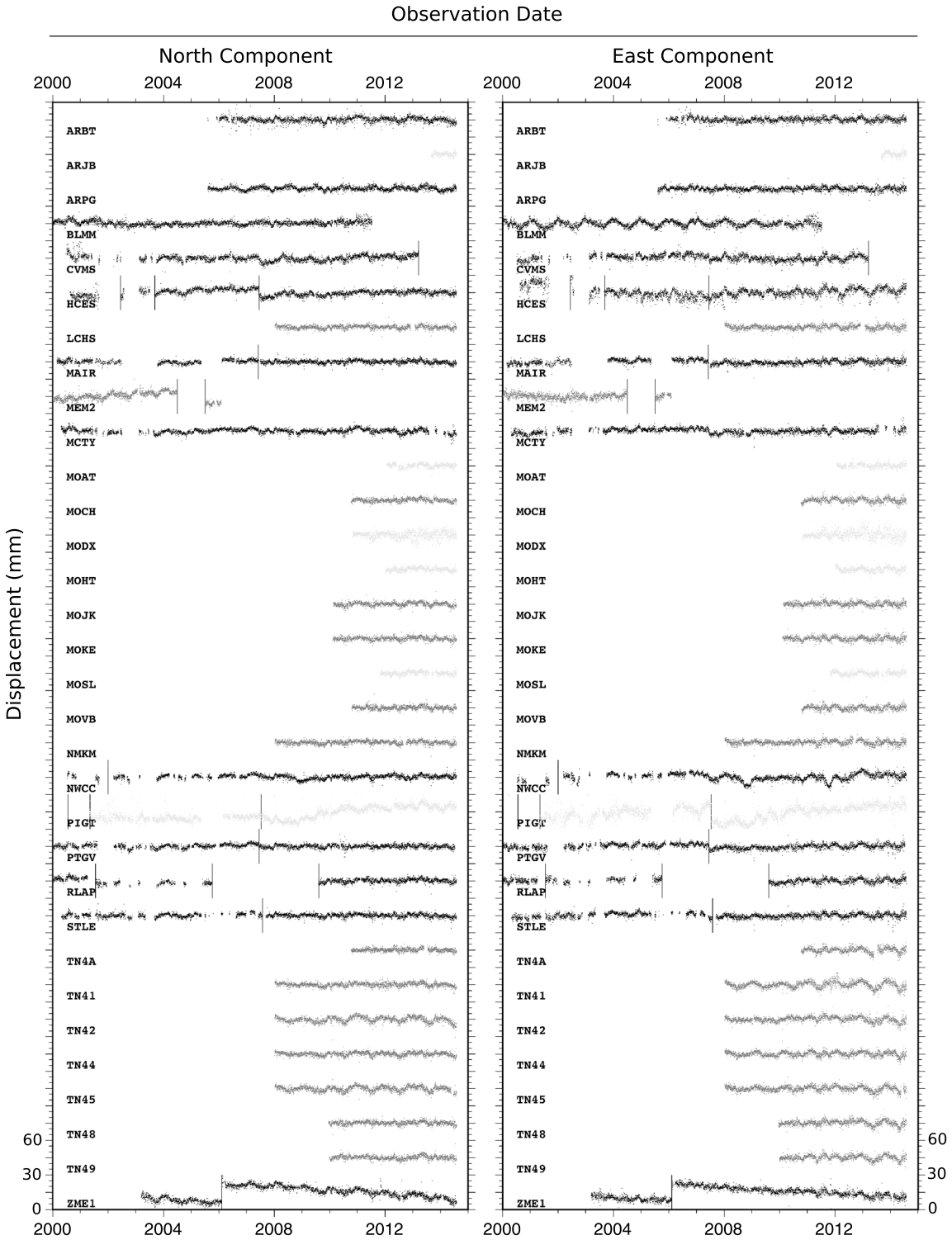

Figure 2. Detrended daily GPS position time series for sites around the NMSZ (purple and blue squares on Figure 1). Horizontal components only are shown. Vertical lines represent breaks in the time series, for which an offset is calculated in the velocity solution. Note that the scales are the same for north and east components. Black time series correspond to those identified as "best" (blue squares, Figure 1). Grey time series are the remaining sites around the NMSZ (purple squares, Figure 1). Time series in light grey are those with <3 years data available which, while included in the velocity solution, are subject to large uncertainties, and so excluded from the subsequent discussion. As discussed in the text, MEM2 and PIGT are also excluded due to local site effects and apparent nonlinearity in the time series, respectively.

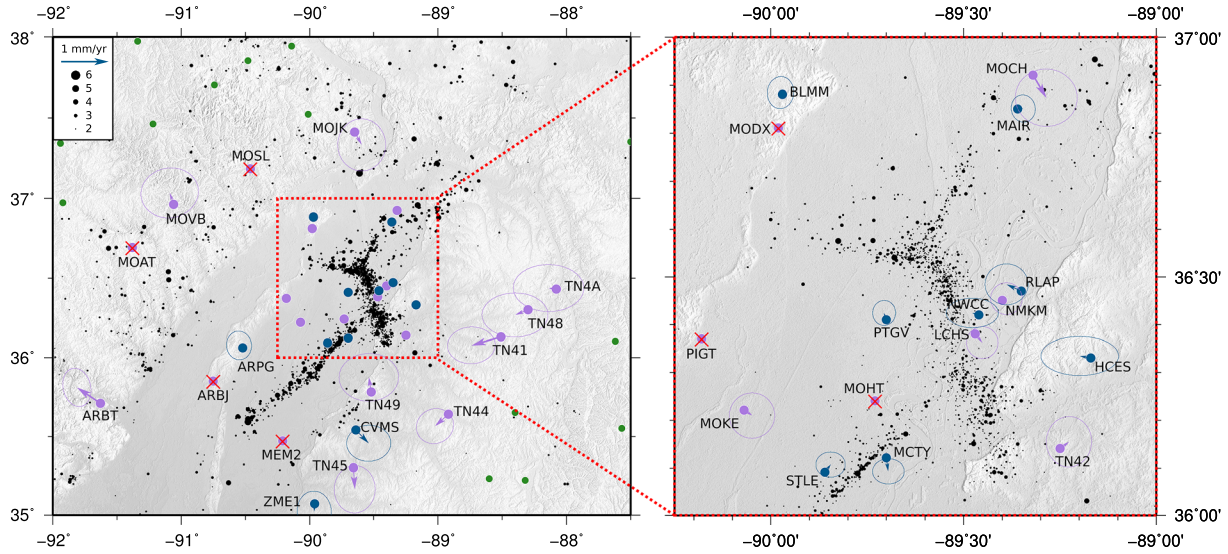

Figure 3. Velocity solution for GPS sites around the NMSZ. Velocities shown are relative to a reference frame defined by fitting a rigid plate to the GPS sites shown in dark blue—those with the longest time series. Error ellipses represent the 95% confidence limit. Red crosses indicate sites removed due to time series <3.5 years in duration (ARBJ, MOAT, MOHT, and MOSL) or due to local site effects as discussed in the text (MEM2, MODX, and PIGT).

in the ITRF2008 reference frame. A Solution INdependent EXchange (SINEX) file with the full covariance information can be obtained from the authors upon request.

4. Strain Accumulation in the New Madrid Seismic Zone

4.1. Velocity Solutions

We use the velocity solution described above to test for the presence of systematic deviations from a purely rigid behavior. This will manifest as a reduced χ^2 significantly greater than 1 and statistically significant residual velocities showing a spatially consistent pattern when these data are fit with a rigid plate model. We exclude from the estimation sites with < 3.5 years of data, in order to minimize the influence of seasonal signals on the velocity estimation [*Blewitt and Lavallée*, 2002]. In addition, we exclude 14 sites which we visually identified as having large residuals ($\gtrsim$ 2 mm/yr) obviously inconsistent with other nearby sites. This leaves a total of 159 sites in the study area. The least squares inversion of their velocities for a rigid plate angular rotation (three parameters) results in a reduced χ^2 of 2.1 and a mean RMS misfit of 0.45 mm/yr. A map view of the residual velocities (Figure S1) shows small residuals overall, in particular, at well-determined sites (i.e., sites with smaller velocity uncertainties), with no discernable spatial pattern. A number of the younger sites show large residual velocities ($\geq$ 1 mm/yr) and similarly large uncertainties, resulting in the relatively large RMS value.

While broadly consistent with little deformation within the plate interior and in agreement with previous large-scale studies [*Calais et al.*, 2006; *Sella et al.*, 2007], the wholesale consideration of such a large area may allow for localized internal deformation, possibly obscured by the statistics of the larger system. We therefore focus on the subset of sites centered around the seismically active NMSZ (blue and purple sites on Figures 1 and 3). Figure 3 shows that residual velocities are very small overall, much lower than 1 mm/yr at most sites and close to zero at several sites, in particular, the sites with the smallest uncertainties.

Site MEM2, south of the Cottonwood Grove fault, shows significant motion to the west relative to other NMSZ sites. However, it is installed on a shallow monument in loose clay (Mississippi embayment "gumbo") known to be sliding downslope (B. Smalley, personal communication, 2010) so that its motion cannot be interpreted in terms of tectonics. Site PIGT shows a high degree of nonlinearity in its position time series (Figure 2), making the determination of a single constant velocity inappropriate. The cause of this nonlinearity is unknown but likely results from local site effects rather than tectonic motion, and so is also excluded from our analysis. Site MODX has a particularly noisy time series (Figure 2) and a short observation duration (<4 years), and we therefore discard it from the interpretation as well.

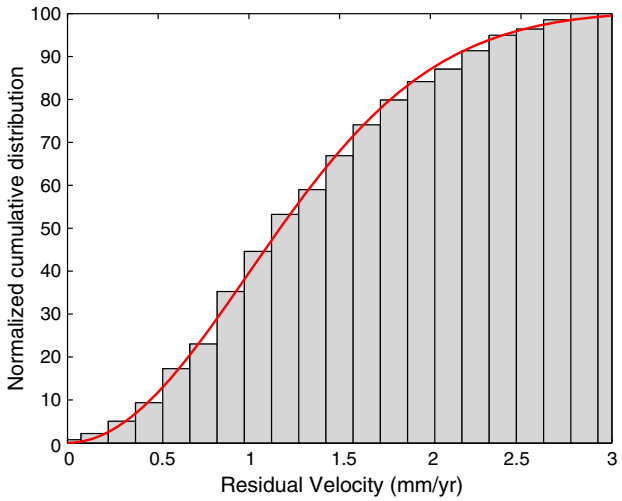

Figure 4. Histogram for the normalized cumulative distribution of velocity residuals (both north and east components) for sites around the NMSZ and WVSZ. The red line shows the theoretical χ^2 distribution expected if residuals are normally distributed in two dimensions with a unit variance.

With the remaining sites, we again search for deviations from a purely rigid behavior by estimating a best fit single rigid rotation of this network and examining residual velocities. Considering only those sites with reliable velocities (25 sites), we find no spatial pattern in their residual velocities with respect to a rigid plate (Figure 3) with an RMS misfit of 0.30 mm/yr (maximum residual of 0.75 mm/yr), and a χ^2 of 1.75, similar to that determined when considering the whole CEUS data set. The same observation holds when velocity residuals are computed with respect to a rigid plate defined using all the Central U.S. network sites processed here (Figure S1). This first-order analysis therefore does not allow us to detect significant deviations from rigid behavior at the level of uncertainty quoted above.

This can be further quantified by testing whether residual velocities follow a normal distribution. Figure 4 shows the cumulative distribution of residual velocities (both in north and east components) normalized by their uncertainty for all sites considered in this and the subsequent section around the NMSZ and WVSZ. This observed distribution is compared to the theoretical χ^2 distribution assuming that the residuals are normally distributed in two dimensions with a unit variance. The excellent fit between the observed and theoretical distributions indicates that the residual velocities are well described by a random process. In addition, the fact that the distribution of normalized residuals is approximately Gaussian validates our noise model and indicates that our probabilistic velocity uncertainties are meaningful.

We then ask whether this conclusion is robust through time, i.e., how residual velocities evolve as the observational data time span increases. We therefore calculate a velocity field for the entire data set based on data initially spanning a time interval from 1 January 2000 to 1 January 2004 and onward, adding incrementally one further year of data each time, and then recalculating the full velocity solution. Sites are included once they have accumulated at least 3 years of observation. We then recalculate the residuals with respect to a rigid plate model defined using the 25 sites around the NMSZ as discussed above, for each time period based on the velocities and their uncertainties available at the end of that time period (Figure 5). As the observation time span lengthens, the east and north velocity residuals for these 25 sites decrease and converge toward zero (note that the inclusion of sites once they accumulate 3.5 years of data results in "new" sites with large residual appearing throughout the sequence). The RMS residual generally decreases (with occasional increases when new sites first accumulate enough data to be included) down to 0.3 mm/yr in mid-2014. Error estimates for individual sites, as expected, generally decrease through time as more data become available and the determination of the time-dependent noise improves. Interestingly, many sites in the initial periods report velocities significantly different from zero and well outside of their estimated uncertainty but, as the duration of their observations lengthens, fall back to be within the uncertainty envelope of zero residual motion. Hence, when attempting to measure submillimetric relative velocities, the reliability of site velocities and the robustness of uncertainty estimates for sites with <10 years of data perhaps becomes questionable.

4.2. Dependence on Site Selection

While the premise of this study is to take advantage of the increased geodetic data available in the Central U.S. to identify small geodetic signals, the quality and duration of the observational time series available is of paramount importance in reducing the uncertainties, which is critical when we are attempting to measure velocities of magnitude smaller than, or comparable to, their uncertainties. Hence, we split our NMSZ group of GPS sites further, and isolate the 11 best sites—those with the longest time series (all with > 8 years, eight with > 11 years) and the lowest noise content. These are identified on Figures 1 and 3 by the dark blue

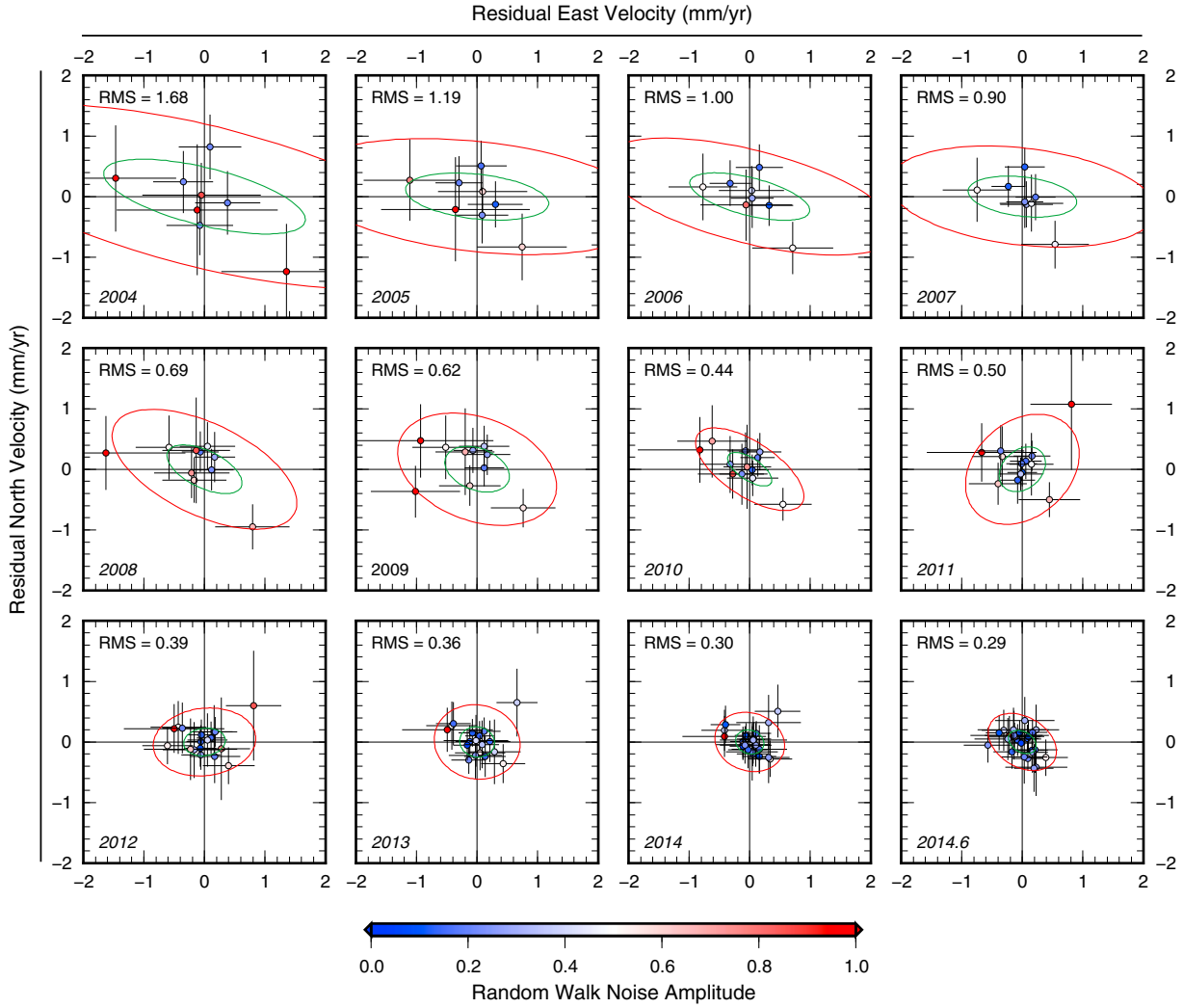

Figure 5. Velocity residuals for each site around the NMSZ (purple and dark blue squares, Figure 1) as a function of observation period. All observation periods start on 1 January 2000 and extend until the start of the year indicated on each panel. Sites are only included in the reference definition, and shown on the figure, once at least 3.5 years of observational data are available. Each point is colored by the magnitude of the random walk noise estimated from the position time series using the FOGMEx algorithm (explanation in the text). Error bars indicate the 95% confidence limit in the site velocity east and north components. Red (respectively green) ellipses on each plot are the contours encompassing the 95% (respectively 39% or 1σ) best fit two-dimensional χ^2 distribution fit to the population of points shown. Values indicated on the top left corner of each panel are the RMS of the magnitude of the residual velocities in mm/yr.

sites, and on Figure 2 by those sites with black time series. When the analysis is limited to this subset of sites around the NMSZ, the picture becomes markedly clearer.

Figure 6 mirrors Figure 5, but using only these 11 sites, and in a reference frame defined using only these sites. Using data covering the 2000–2004 time period only, four of the nine sites present have a residual velocity with 95% error bars on the EW and NS components that do not encompass zero. Once the time period is extended to 2000–2014, all 11 sites present have a residual velocity with 95% error bars that now encompass zero, with an RMS of the residual velocities of 0.21 mm/yr and a reduced χ^2 of 1.48. Sites RLAP, HCES, and CVMS are consistent outliers (indicated by their first initial on the tenth panel of Figure 6), although their NS and EW error bars encompass zero for the whole 2000–2014 time period. RLAP is characterized by a long time series hindered by a significant data gap and a number of other discontinuities (Figure 2). The time series for HCES shows a relatively large amplitude of time variable noise, likely explaining the increased residuals. CVMS presents a complex case for the assessment of its noise content and uncertainties and is considered in detail later (see section 6). We also observe (particularly starting with the 2010 panel of Figure 6) that sites with the best quality time series, i.e., with the lowest colored noise (blue circles

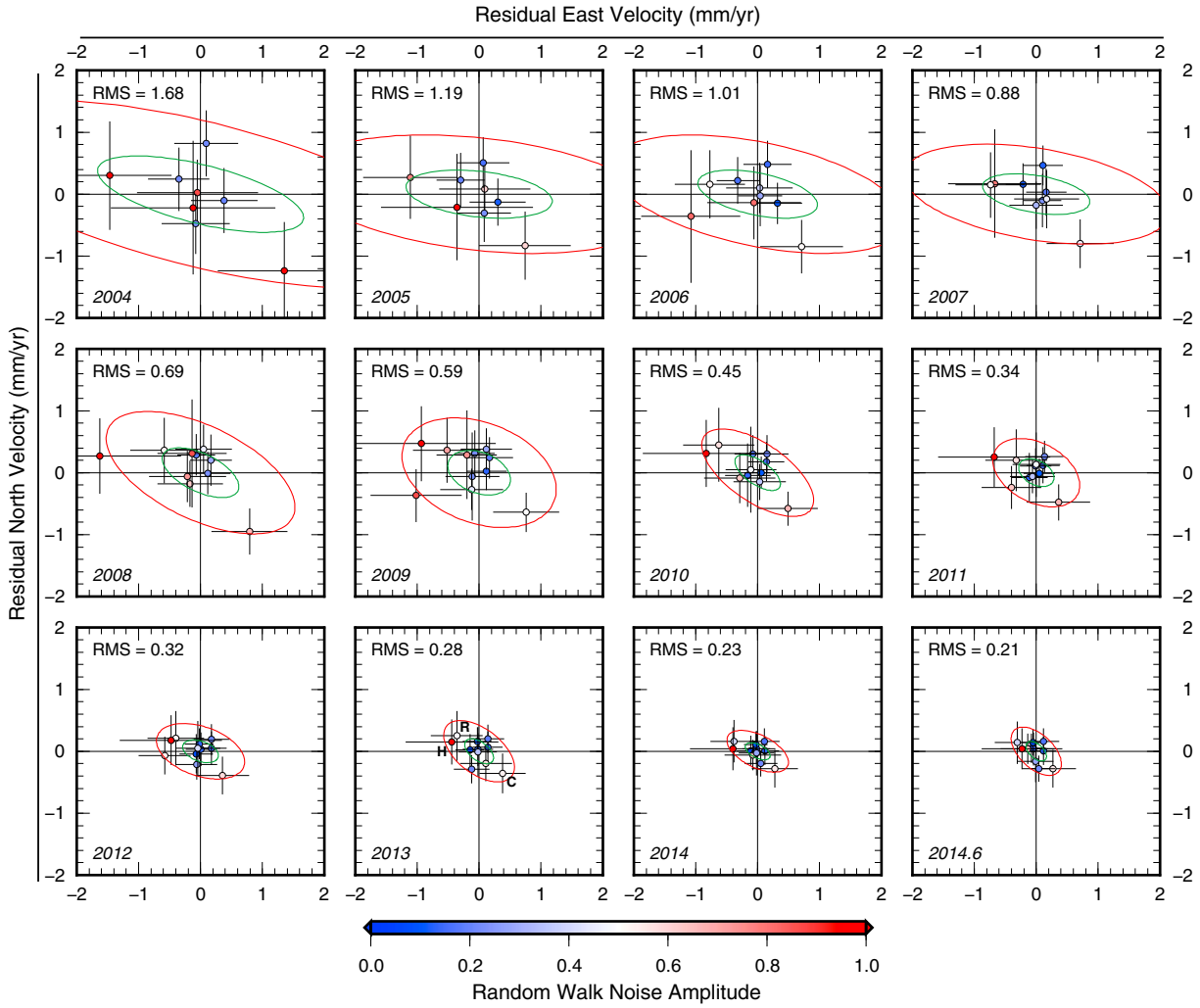

Figure 6. As in Figure 5, but limited to the best 11 sites around the NMSZ (dark blue squares, Figure 1), and in a reference frame relative to those 11 sites.

on Figure 6), have residual velocities closest to zero, while sites with higher colored noise tend to remain outliers (e.g., sites RLAP, HCES, and CVMS).

Finally, we observe on Figure 6 that the ellipses encompassing the 95% and 1σ two-dimensional χ^2 distribution fit to the population of velocity residuals decrease continuously as the time series duration increases. This is further illustrated on Figure 7, which summarizes the dependence of the mean residuals and their confidence limits on the duration of the observation period. The best constrained result for the 11 best sites around the NMSZ, in a frame defined by those sites (Figure 7), has a mean residual of 0.18 mm/yr, within the mean 1σ confidence interval of zero deformation (based on averaging both the semiaxes of the individual uncertainty ellipses), and with an upper limit to the 1σ confidence interval of 0.21 mm/yr. This is similar to, although a slight improvement on, that determined by *Calais and Stein* [2009] of 0.2 mm/yr, although more sites and longer time series are used here.

The choice of sites used in the reference frame definition does not significantly influence the resulting residual velocities, for these 11 sites are not significantly different to those resulting from using the frame defined using all the sites around the NMSZ, or all those in our CEUS network, reinforcing the initial statement of this section that the principal motion of the large majority of our sites in the Central US can be adequately fit by the motion of a single rigid plate.

Mean residual velocities first decrease as a function of time as the observational time series for many of the newer sites around the NMSZ are augmented by new data, but then appear to flatten out at around

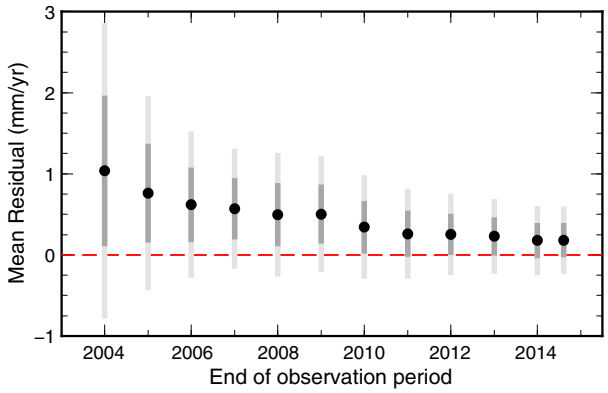

Figure 7. Mean residuals and confidence limits for deformation across the NMSZ as a function of observation period duration, for the best 11 sites around the NMSZ, relative to a rigid plate defined using only these sites. Black circles indicate the mean residual relative to behavior as a rigid plate, the dark grey bars indicate the mean 1σ uncertainty interval, and the light grey bars the mean 95% uncertainty interval. The horizontal red line highlights zero deformation. The *x* axis indicates the end of the observation period.

0.2 mm/yr after ~10 years of observation (Figure 7). The 95% uncertainty however always includes zero, as well as the 1σ uncertainty in the later part of the time interval considered here. The inclusion of data from 2012 in fact leads to a slight increase in the overall residuals, likely due to an enhanced noise content in the data from that year (see section 6 for more on this issue) or the influence of some nontectonic transient displacement in this year.

Further refinement of this 0.2 mm/yr limit is challenging, although the best set of sites used does continue to show an increase in precision with time, though at a decreasing rate (Figure 7). That longer time series and more sites do not significantly improve the uncertainty suggests that we are at the detection limit of what is possible to achieve after 14 years of observations within our current understanding of the noise content in GPS time series and of the influence of nontectonic (e.g., seasonal hydrological) deformation on our data. It is interesting to note that the inclusion of large numbers of new sites, while greatly improving the spatial coverage of such geodetic surveys, does not impact upon the best limit achievable, which is derived using only those sites local to the study area with the longest time series, in their own self-defined reference frame. This emphasizes that the most precise constraints on strain are derived from using limited higher-quality sites, with >10 years of observational data and that, for local applications, the realization of a simple local reference frame is sufficient.

4.3. Baseline Length Changes

We have shown so far that there is no systematic pattern in GPS velocities in the NMSZ that could indicate a significant deviation from purely rigid behavior and that, on the whole, current deformation does not exceed 0.2 mm/yr. While this lack of regional deformation limits any large-scale strain, extremely localized strain arising from a focused geodynamic influence remains a possibility. For instance, *Frankel et al.* [2012] assessed east and north relative motion between individual site pairs and concluded that there was resolvable localized motion between site STLE and four other continuous GPS sites in the broad New Madrid region (CJTR, MACC, MAIR, and PTGV) at rates up to ~0.4 mm/yr. The possibility of localized deformation therefore remains, with the potential to add an extra constraint to the various suggested models to explain the occurrence of seismicity in the NMSZ.

To test this possibility, we calculate the rates of horizontal baseline length change between all sites in the NMSZ network and between the 11 best sites around the NMSZ (Figure 8). Baseline lengths are invariant to a rigid rotation of the network, whereas the north and east components of the baselines are not and should therefore be used with caution when interpreting strain within a network. While the differencing of positions for a site pair in principle increases the noise content of the resulting baseline time series relative to the position time series of each individual site, it also effectively removes spatially correlated signals in the time series (such as those likely to result from long-wavelength hydrological loads) when the site spacing is small relative to the spatial wavelength of the common signal. All baseline lengths and rates shown and discussed herein are for horizontal motions only, and do not incorporate the vertical component. We calculate the rates of baseline length change by fitting the best linear trend to the baseline time series, allowing for offsets at times when instrumentation changes or obvious discontinuities in the time series occur. Examples are shown in Figures 8 and S4.

We expect that some baseline length rates-of-change will be nonzero, either as a result of tectonic or nontectonic processes. If they result from a regional tectonic processes rather than a site-dependent issue, then a spatially systematic pattern should emerge. This will manifest as a non-Gaussian, noncentered

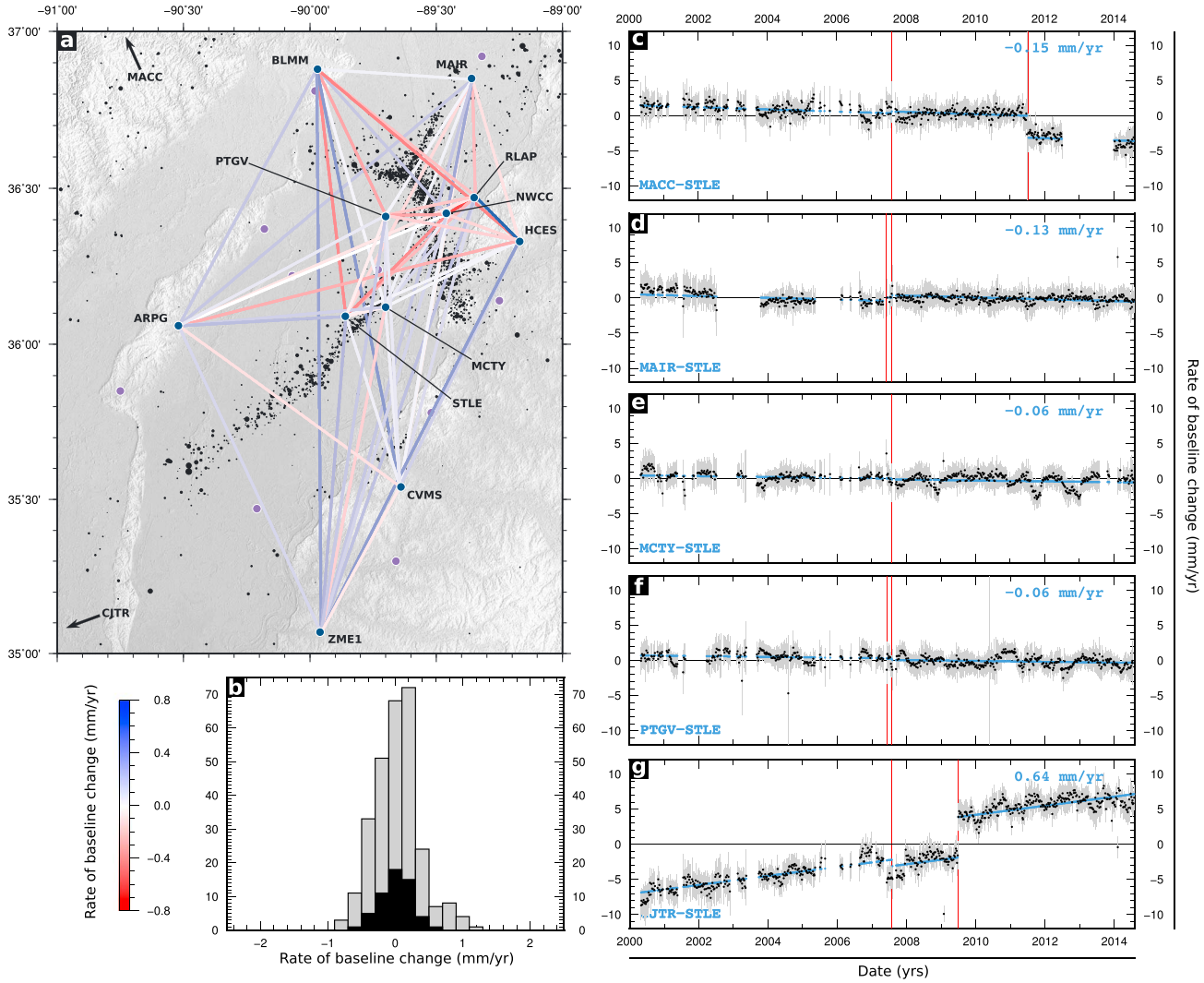

Figure 8. (a) Map showing baseline rates of change for all site pairs between the best 11 NMSZ sites. Rates are indicated by the coloring of the line connecting sites. Selected examples are shown in Figures 8c–8g and in Figure S3. (b) Histogram of all baseline rates of change for all site pairs in the NMSZ subnetwork with at least 3 years of data. Black bars are for those site pairs where both sites are included in the 11 best sites. (c)–(g) Variations in baseline length between STLE and five sites used in *Frankel et al.* [2012]. In each case, the mean baseline length has been subtracted. MACC is located to the NNW of the NMSZ, and CJTR to the SW, off the map in the directions indicated. Black points are baseline lengths, with grey bars indicating the 95% confidence level. Blue points are the best fit linear trend, with vertical red lines indicating breaks in the time series, where an unconstrained offset in the time series is applied during the determination of the rate. Labels indicate the site pair and the rate of length change.

distribution of the baseline length rates-of-change. Conversely, a Gaussian distribution centered on zero reveals a lack of systematic pattern and disproves, at the uncertainty level of the distribution, the existence of strain within the network. As Figure 8b shows, the full distribution of baseline length rates of change shows a Gaussian distribution centered on zero, with a slightly larger standard deviation when considering all sites (grey bars) than only the 11 best ones (black bars). Only two of the baselines between the best 11 sites show length changes greater than 0.4 mm/yr (NWCC-RLAP and HCES-RLAP). This is however an artifact of their low-quality differenced time series, as shown on Figure S4, lower left panels. Therefore, no consistent pattern "emerges" from this analysis of baseline length rates-of-change, a reference frame-independent quantity. This is corroborated by the visual inspection of the baseline map on Figure 8.

Baseline length time series and their rates of changes for the five site pairs reported in *Frankel et al.* [2012] are shown in Figures 8c–8g. In our analysis, incorporating 4 years of extra data, only CJTR-STLE has a rate of change significantly different to zero. Site CJTR is located on bedrock at the southwestern edge of the Mississippi Embayment, over 200 km from the seismically active region of the NMSZ. While its motion is

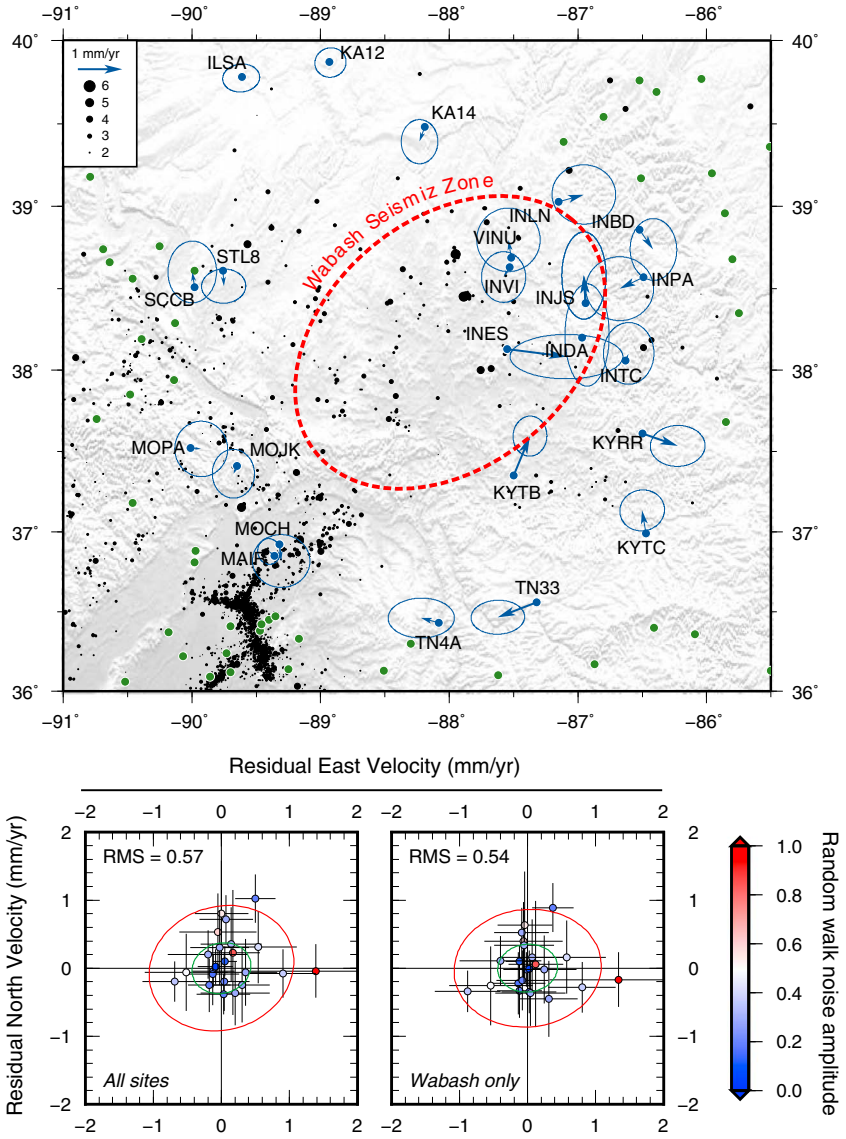

Figure 9. (top) Velocity solution for GPS sites around the WVSZ. Velocities shown are relative to a reference frame defined by fitting a rigid plate to all the GPS sites shown in Figure 1b. Error ellipses represent the formal 95% confidence limit. (bottom) Velocity residuals for sites in the WVSZ relative to a reference frame defined using all the GPS sites shown in Figure 1 (as in Figure 9, top). Points are colored by the magnitude of the random walk noise. Error bars indicate the 95% confidence limit. Red (respectively green) ellipses on each plot are the contours encompassing the 95% (respectively 39% or 1σ) best fit two-dimensional χ^2 distribution fit to the population of points shown. Values indicated at the top left corner of each panel are the RMS of the magnitude of the residual velocities in mm/yr.

consistent with significant extension between it and the central NMSZ (represented by STLE), it may not be representative of the overall tectonics of the region. Notably, site ARLR, located just to the south of CJTR, shows a velocity relative to our regionally defined plate within error of zero and significantly different to that at CJTR, despite its proximity (Figure S1).

5. Strain Accumulation in the Wabash Valley Seismic Zone

The majority of GPS sites in the WVSZ (Figure 1b) have time series of 4 to 6 years duration (Figure S2). This is substantially shorter than most of those available in the NMSZ, and hence, velocity uncertainties are significantly higher (Figure 9).

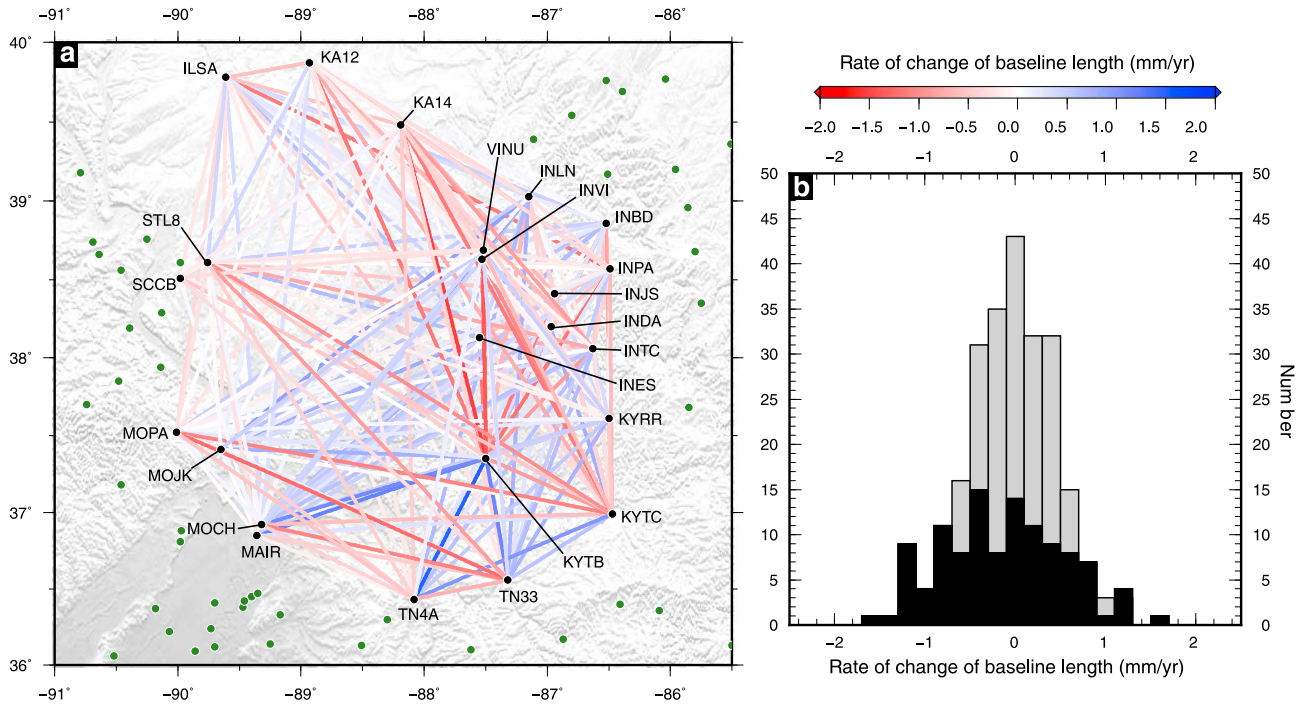

Figure 10. (a) Maps of baseline length rates of change for all sites around the WVSZ with >3.5 yrs of data. Lines linking site pairs are colored by rate. (b) Histogram of baseline length rates of change for all site pairs with > 3.5 yrs of data. Black bars are for those site pairs including the five sites from Figure 9 with residuals beyond their 95% confidence limit from zero (INES, KYTB, KYTC, KYRR, TN33). Example baselines are shown in Figure S4.

Using the same analysis routine, in which residual velocities for sites around the WVSZ are considered relative to a self-defined reference frame, five of the 24 sites around the WVSZ show velocities outside of their 95% confidence limit from zero (Figure 9, top). However, there is no coherent pattern present in the residual site velocities. The full data set for the WVSZ, including these five sites, fits zero motion with a mean residual of <0.6 mm/yr. Shifting from the regional reference frame to the local WVSZ reference frame produces only a small (0.04 mm/yr) decrease in the RMS residual. We note that four of the five sites with residual velocities outside their confidence interval are monumented on steel pillars anchored in masonry—a suboptimal setting for the level of precision required for tectonic geodesy. Given the lack of coherent deformation and the generally good fit to the zero-motion hypothesis displayed by the majority of sites, we ascribe the residuals at these five sites to local monument instability, rather than regional tectonics.

The lack of coherent deformation in these results does not support earlier interpretations based on the results of campaign GPS data, which, on the basis of a consistent subuncertainty trend in velocities, suggested an overall approximately NE-SW extension across the WVSZ [*Galgana and Hamburger*, 2010]. No such pattern is present in the continuous velocity solution presented here, above the level of uncertainty present in our results. To investigate this issue in more detail, we computed horizontal baselines length changes for all WVSZ network baselines (Figure 10). As with the NMSZ, the distribution of these measurements appears Gaussian and centered on zero, with very few site pairs with baseline length changes in excess of 1 mm/yr, other than those involving sites KYTB and INES (included in the black bars on Figure 10b). Several baselines extending across the WVSZ from NNE-SSW show extension at very slow rates (<1 mm/yr, often <0.5 mm/yr) such as INLN-MOJK for example (Figure S4, bottom center panel). Such baselines are however contradicted by similarly trending ones with near-zero length changes (e.g., INPA-MAIR/MOJK, INBD-MOJK) or slight contraction (e.g., KA14-MOPA/TN4A).

Altogether, the WVSZ data set analyzed here does not present evidence of a significant or consistent deviation from a purely rigid behavior at the ~0.6 mm/yr level or significant motion with respect to the rest of the CEUS.

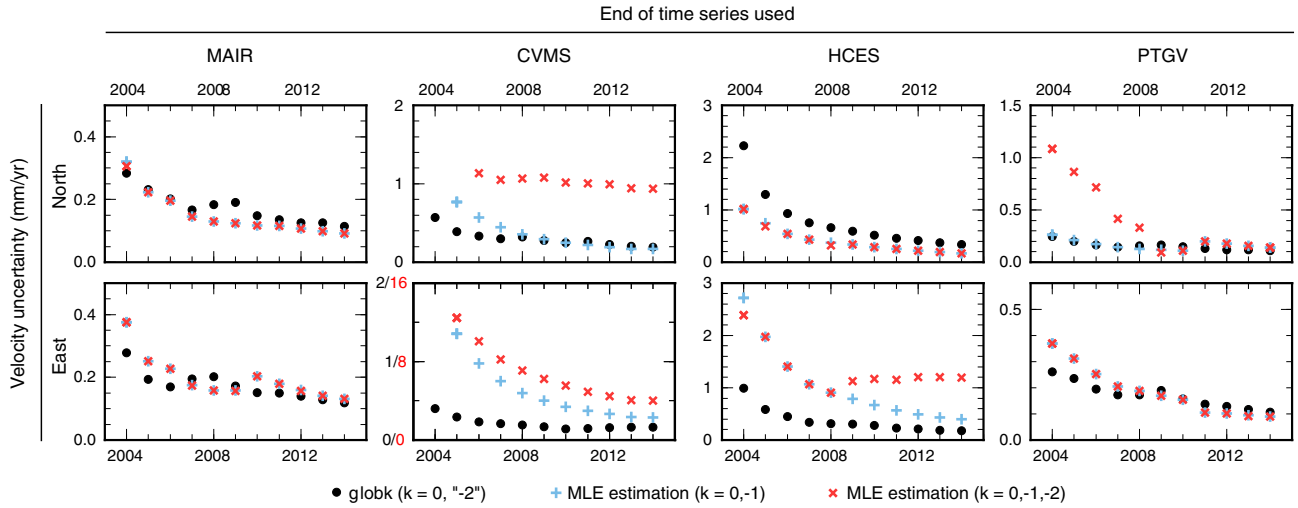

Figure 11. Uncertainties as a function of time series duration for different models. Each panel shows uncertainties for three different noise models, determined using the available time series from the start of 2000 up until the date at which the point is shown. Black points are determined using the method described *Reilinger et al.* [2006], wherein noise is characterized as a combination of white noise and a random walk process. Blue crosses are for a combination of white and flicker noise [*Williams*, 2008], and red points are for a combined white, flicker, and random walk noise model [*Williams*, 2008]. For the east component of site CVMS, the velocity scale is different for the black and blue points (black annotations) and the red points (red annotations).

6. Influence of Noise Models on Uncertainty Estimates

We now ask whether the conclusions presented above would be altered by using a different strategy to compute velocity uncertainties. The method employed in this study involves the extrapolation of the position time series to an infinite duration in order to assess the time variable noise content of the time series as a combination of white noise and a random walk using the FOGMEx algorithm of *Herring* [2003]. We compare the uncertainties estimated using this method with those calculated using the maximum likelihood estimation method of *Williams* [2008], which explicitly fits the time series power spectra with a set of noise models incorporating different combinations of white, flicker, and random walk noise [*Williams*, 2003; *Langbein*, 2004].

Figure 11 shows the results of this comparison for four of the sites around the NMSZ—MAIR, CVMS, HCES, and PTGV. In each case, we calculated uncertainties for time intervals of increasing duration and for three noise models. Uncertainties are only calculated where enough data are present for the noise processes to be appropriately estimated. As expected, uncertainties generally decrease as the time series duration increases, until the estimated uncertainty reaches ~0.2 mm/yr. At this point the addition of a further year of data can either lead to an increase or decrease of the uncertainty depending on the noise content of that specific year, as best illustrated by sites MAIR (2007–2008) and PTGV (2008–2009) on Figure 11. The overall agreement between the FOGMEx method used here and the explicit maximum likelihood estimation of white/flicker or combined white/flicker/random walk noise is generally very good, in particular, as the time series durations increase. When there are significant differences, our estimated uncertainties are usually lower than those using an explicit noise model. Therefore, our interpretation of a lack of detectable deformation in the CEUS would also hold, had we used an explicit colored noise model (flicker or random walk).

While in many cases the various noise models produce very similar uncertainties (e.g., MAIR, HCES north component, and PTGV east component), there are cases with major differences. This is illustrated by site CVMS on Figure 11, where the difference between the white-flicker-random-walk noise model and the other two models is a factor of ~4 on the north component, and ~8 on the east component (note the different scale used). We suspect that this behavior is the result of some currently unexplained site-specific complexity in the spectral makeup of the noise content of the data at this site.

As mentioned in section 4.1, the position time series for site MODX is visually noisier (Figure 2), with a much greater velocity uncertainty than other sites. To test the degree to which this noise can influence our velocity solutions and, in particular, the uncertainty estimates, we redetermined uncertainties using noise models

incorporating white/flicker, white/flicker/random walk, and white/random walk noise by maximum likelihood estimation [*Williams*, 2008]. With each noise model, the estimated uncertainty was at least a factor of 2 greater than that estimated using the routine method outlined above, and in the case of the white/random walk model, exceeded 5 mm/yr. As a result, we feel justified in excluding this site from our analysis until further data become available to better constrain the noise model required and the resultant velocity.

7. Discussion

7.1. Detectable Deformation in the NMSZ and WVSZ?

We have established above that the level of currently available GPS data in the NMSZ shows no demonstrable evidence for internal deformation at rates above 0.2 mm/yr, corresponding to a maximum strain rate of $\lesssim 10^{-9}$ yr^{-1} over the width of the NMSZ, consistent with the earlier findings of *Calais and Stein* [2009]. These values represent an upper bound, as both the velocity across the region is an upper bound and the scale over which it takes effect is a lower bound. We were however unable, with four additional years of data, to confirm the results presented in *Frankel et al.* [2012] of significant motion between selected GPS sites in the NMSZ. For the WVSZ, we also find indiscernible deviation from rigid behavior ($\lesssim$0.6 mm/yr) with present-day strain rates limited to $\lesssim 1–2 \times 10^{-9}$ yr^{-1}. The latter result is similar to the findings of *Hamburger et al.* [2002] and *Galgana and Hamburger* [2010], who also found little evidence for significant internal deformation based on three campaign GPS measurements spread over a period of 11 years, at levels greater than their uncertainties.

We further test the null hypothesis that the data fit a model with zero strain rate by generating simulated time series for the 11 best NMSZ sites based solely on their noise content (white + time dependent, as determined using the FOGMEx method discussed above; [*Herring*, 2003; *Reilinger et al.*, 2006]), with a zero-velocity background at all sites. We sample these synthetic time series at the epochs of the actual observations for each site and estimate a velocity using a least squares fit to the resulting simulated time series. We compute 1000 such simulated time series for each site and test whether the observed velocities (based on the final epoch of Figure 6) can be distinguished from measurement noise. As shown on Figure 12, observed velocities are in all but one case within the 95% confidence interval defined by the noise-only simulations (the single marginal exception being for site ARPG). We therefore conclude that the currently available GPS data in the NMSZ does not allow us to confidently detect motions different from zero at the precision level of the data.

As longer time series become available, it may be possible to improve the precision of the GPS measurements below the current limit of 0.2 mm/yr, as shown on Figure 7 which in turn may allow for the detection of deformation in the NMSZ. However, this will require more high-quality sites in order for (1) a spatially coherent pattern indicative of actual tectonic deformation to emerge from the measurement noise and (2) statistics to confidently show that the null hypothesis of purely rigid behavior can be discarded.

7.2. Implications for Intraplate Seismicity

The absence of resolvable deformation across the NMSZ—a region that has experienced a sequence of large earthquakes in the past few thousand years—poses a number of questions. Is the historical seismicity as well as the currently recorded activity evidence for present-day strain accrual in a fault system that is at steady state in the Holocene [*Hough and Page*, 2011]? In that case the rate of strain accrual measured geodetically should be consistent with the Holocene rate of strain release by earthquakes. Or has a recent change in the regional stress field triggered the release of strain that accumulated some time in the geological past [*Calais et al.*, 2010] with fault systems behaving in a time-dependent manner? That hypothesis would be consistent with a mismatch between the rates of strain accrual and release during the Holocene and with current seismicity in the NMSZ being a long-duration aftershock sequence of the 1811–1812 events [*Stein and Liu*, 2009], rather than the result of present-day strain accrual, as suggested by *Page and Hough* [2014].

To address this issue, one can compare the (upper bound) rate of strain accumulation determined above with the rate at which strain would need to be released by earthquakes of a given magnitude over a given area, should the system be at steady state. This is classically done for deforming regions using *Anderson*'s [1979] relation between strain rate and seismic moment rate for an areal zone and assuming that seismicity follows a Gutenberg-Richter distribution. Here instead of assuming the area over which strain is accumulating—an unknown quantity unless the strain accumulation mechanism process is known—we vary it to find the range of resulting recurrence times permitted by the data (Figure 13a).

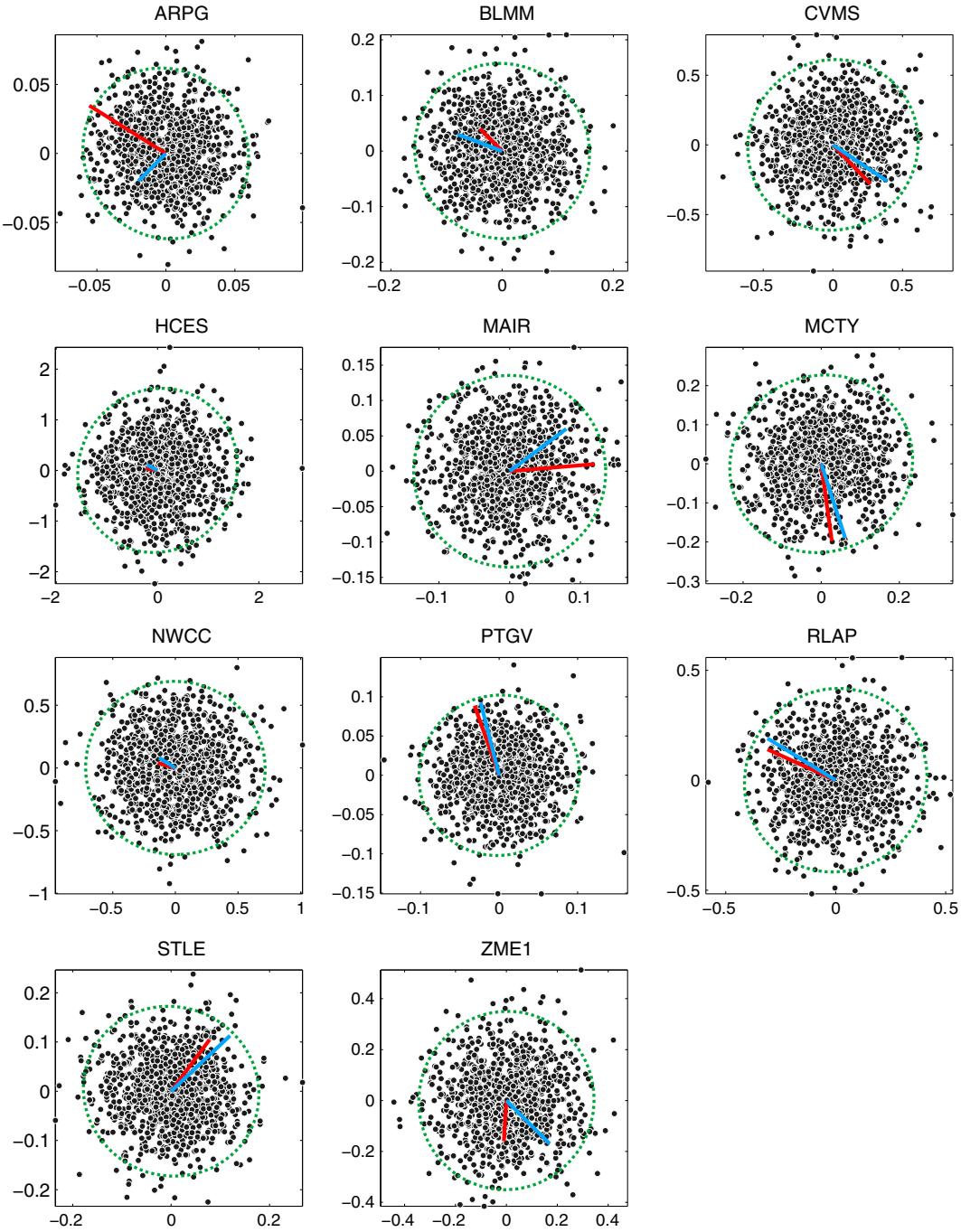

Figure 12. Velocities at the 11 best NMSZ sites (black points) from 1000 simulated time series that assume zero velocity and the white and colored noise content estimated from the actual time series. The green dashed contour is calculated to encompass 95% of the simulated velocities. The colored bars show the velocities estimated from the actual data (Figure 3) with respect to a rigid plate estimated form the best NMSZ sites (red) and the entire CEUS network processed here (blue).

Paleoliquefaction events in the NMSZ region indicate that the area has experienced severe seismic shaking approximately every 500 years during the late Holocene [*Tuttle et al.*, 2002, 2005]. Taking this recurrence time for the New Madrid area, a strain rate of 10^{-9} yr^{-1} implies, for M_w 6.8–7.0 earthquakes [*Hough et al.*, 2000], an area of 40,000–100,000 km^2. This is consistent with *Hough and Page* [2011] who assumed an area of 20,000–40,000 km^2 on the basis that it was the domain size in the flexural postglacial rebound model of *Grollimund and Zoback* [2001]. If we use instead the area over which horizontal strain caused by Glacial

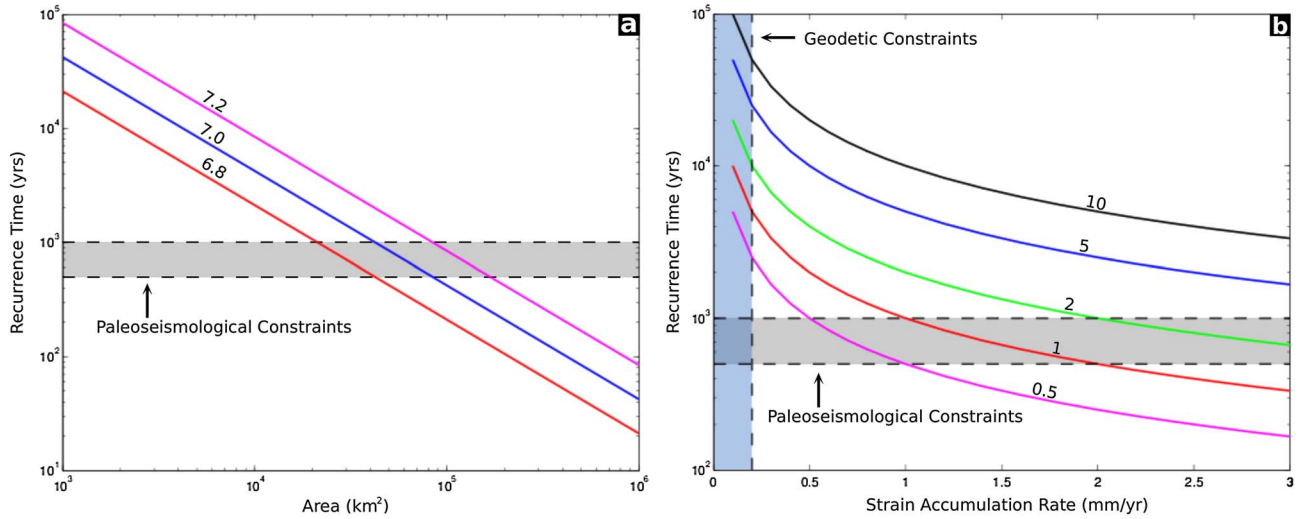

Figure 13. (a) Recurrence time as a function of the area over which strain is accumulated. Lines are calculated using the method of *Anderson* [1979] for different maximum magnitudes, as indicated by their labels. The grey region indicates the recurrence time determined by paleoseismic studies of liquefaction in the New Madrid region. (b) Recurrence time as a function of strain accumulation rate, for earthquakes of different coseismic slip. Lines are calculated for the slip on the fault during an earthquake, as indicated by their labels, which are given in meters. The grey-shaded area indicates the recurrence interval from paleoseismic studies. The blue-shaded area indicates the strain accumulation rate permitted by geodetic observations.

Isostatic Adjustment is actually observed in the Central and Eastern U.S. [*Calais et al.*, 2006; *Sella et al.*, 2007], $\sim 6 \times 10^6$ km^2, we then obtain a recurrence time less than 50 years, inconsistent with observations of seismicity across the same areal extent. Conversely, invoking a local process such as strain accumulation on the Reelfoot Fault [*Frankel et al.*, 2012] would imply a recurrence time of several thousands of years, inconsistent with paleoseismological observations. Finally, using the area over which strain is currently released by earthquakes in the NMSZ (~10,000 km^2) leads to a recurrence time of 2,000–4,000 years for M_w 6.8–7.0 events, again inconsistent with paleoseismological observations.

Such scenarios, and many others possible, can be justified either a priori (because it relies on a plausible strain accumulation process) or a posteriori (because it leads to the observed late Holocene recurrence time). However, none of them is satisfactory since *Anderson*'s [1979] equation assumes that the volume over which strain is released is the same as the volume over which it is accrued. It also assumes that the fault system is at steady state, as observed at plate boundaries. The validity of these assumptions in the case of the CEUS is uncertain because we do not know the size of the region that is currently straining or the length scale of the process loading faults, and because the steady state behavior of intraplate faults such as the New Madrid system remains to be demonstrated, as discussed below.

7.3. Evidence for Time Variable Deformation

An alternate way to compare strain accumulation and release is to make the simple assumption that interseismic far-field motions (a maximum of 0.2 mm/yr for the NMSZ) result in strain accrual on a single fault, with no creep, to be released in earthquakes of a given magnitude. This reasoning is often used at plate boundaries to determine the potential earthquake magnitude on a given fault segment knowing the strain accumulation rate (usually termed "slip rate") and the time since the last major earthquake on that segment. As shown on Figure 13b, a fault that steadily accrues strain at 0.2 mm/yr should, in steady state, release one *M7* earthquake every 3000 years or more. Estimates of the magnitude of the 1811–1812 earthquakes vary, with the most recent work favoring the range 7.0–7.5 [*Hough et al.*, 2000] while earlier results favored magnitudes 7.8–8.1 [*Johnston*, 1996]. In that latter case, 0.2 mm/yr of deformation in the NMSZ would imply an earthquake repeat time greater than 10,000 years.

Liquefaction features triggered by ground shaking show that earthquakes similar in magnitude and location to the 1811–1812 events occurred at 1450 ± 150 C.E. (Common Era), 900 ± 100 C.E., 300 ± 200 C.E., and 2350 ± 200 B.C.E. (before the Common Era) [*Tuttle et al.*, 2005]. This amounts to an average occurrence time of 500 years for the past three cycles, an order of magnitude shorter than predicted for a steady state fault loaded at the maximum rate allowed by the geodetic data. Further back in time, geomorphic studies show

that the course of the Mississippi river was straightened by an earlier sequence of events between about 2200 and 1600 B.C.E. [*Holbrook et al.*, 2006]. Liquefaction features indicate a 2350 ± 200 B.C.E. event [*Tuttle et al.*, 2005], coincidental with the beginning of the straightening sequence. If all these events were similar in magnitude to the 1811–1812 earthquakes, the average repeat time since the Middle Holocene would be on the order of 900 years (assuming a minimum of one event per cluster), still much shorter than what the geodetic data require at steady state. If some large events have been missed in the paleoseismological record, the discrepancy between paleoseismological and geodetic estimates of earthquake repeat times would be even greater.

However, the comparison between earthquake recurrence from paleoliquefaction observations and from geodetic measurements of strain accumulation rates must however account for the fact that the liquefaction data do not precisely determine the spatial extent of each earthquake rupture. In addition, several earthquakes closely spaced in time may appear as a single liquefaction event. As such, two liquefaction events recorded at the same site may in fact record earthquakes on consecutive segments of fault, rather than a repeat earthquake on the same fault segment. This being the case, the comparison of such paleoseismological data with geodetic estimates of present-day strain and subsequent interpretation in terms of slip rate estimates on specific faults, must be treated with caution.

The simplifying assumption used above, that strain would accrue on a single NMSZ fault, is of course improbable given observations of recent faulting elsewhere in the midcontinent. Paleoseismological records indicate shifts in the locus of the largest earthquakes from the Fluorspar Area fault complex in southern Illinois to the NMSZ in the past several 10,000 years [*Potter et al.*, 1995; *McBride et al.*, 2002]. The Saline River fault in SE Arkansas shows evidence for multiple large earthquakes in the Holocene [*Cox et al.*, 2000] as does the Meers fault in Oklahoma, with two surface-rupturing earthquakes in the past 3000 years [*Crone and Luza*, 1990]. Distributed faulting, as indicated by the paleoseismological record, would however imply a recurrence interval even longer than 3000–10,000 years assuming steady state behavior of midcontinent faults.

Strain in the NMSZ is therefore accumulating at present at a rate that is too low to account for the known large earthquakes of the past ~5000 years. Taken together, the geodetic and paleoseismological data therefore exclude steady state fault behavior over that time period. This implies that either the rate at which the NMSZ is loaded, its mechanical strength, or both, vary with time. This time dependence of the fault behavior may explain the apparent "clustered and migrated" nature of earthquakes in plate interiors [*Crone et al.*, 2003], a feature previously recognized in the CEUS [*Wheeler and Crone*, 2001].

8. Conclusions

The analysis of continuous GPS data collected over a 14.6 year interval in the Central Eastern United States shows no detectable geodetic strain above the level of uncertainty in the data. Around the NMSZ, sites with the longest observational record show no significant deviation from the behavior of a rigid plate with a mean residual of 0.17 mm/yr. This is equivalent to an upper bound of $\lesssim 10^{-9}$ yr^{-1} on the present day strain rate across the NMSZ. Around the WVSZ, continuous GPS observations limited to a 4–6 year time period show a similar behavior with a mean residual of ~0.6 mm/yr. Consideration of baseline length rates of change between stations in the NMSZ or WVSZ similarly shows no coherent or significant pattern of deformation.

Geodetic and paleoseismological data, when taken together, show that the (maximum) rate at which strain currently accumulates in the NMSZ is much lower than the rate at which it has been expended in large earthquakes during the Holocene. This conflict between the rates of strain accrual and release excludes the possibility of steady state fault behavior and implies that fault loading, fault strength, or both must vary with time. For instance, stress changes caused by erosional unloading is a mechanism capable of triggering earthquakes on faults with favorable orientations [*Calais et al.*, 2010]. Hydrological processes have also been shown capable of triggering significant earthquakes by increasing pore fluid pressure either naturally [*Bollinger et al.*, 2010] or as the result man-made fluid injections [*Keranen et al.*, 2013]. Alternate mechanisms may bring intraplate faults to failure, such as fault stressing by aseismic slip in the lower crust [*Frankel et al.*, 2012], a process yet to be documented directly. Stress changes due to GIA likely play a role in intraplate faulting, but at higher latitudes, as their magnitudes decay rapidly away from the former ice margin and are too small to single-handedly account for faulting in the NMSZ [*Wu and Johnston*, 2000].

The very low strain rates found here in the NMSZ, although insufficient to load individual faults at a rate consistent with the observed recurrence of large Holocene earthquakes, however, do not rule out the possibility of large earthquakes on other faults in the midcontinent, as the Quaternary paleoseismological record indicates.

Acknowledgments

We thank the Editor, one anonymous reviewer, and Robert W. King for their careful comments on the manuscript. This work uses data services provided by the UNAVCO Facility with support from the U.S. National Science Foundation (NSF) and National Aeronautics and Space Administration (NASA) under NSF Cooperative agreement EAR-0735156. E.C. was supported in part by USGS grant G10AP00022. T.J.C. was supported by an ENS postdoctoral fellowship. We thank the IGS and its centers for providing open GNSS data and data products to the community. All data used in this work are openly available from the CORS (http://www.geodesy.noaa.gov/CORS) and UNAVCO (http://www.unavco.org) archives. Ancillary information necessary to process GPS data, such as precise satellite orbits and antenna phase center models are openly available from the IGS (http://www.igs.org). Global SINEX files used here are available at MIT (http://acc.igs.org/reprocess.html). The software used to process the GPS data (GAMIT-GLOBK) was used under licence from the Massachusetts Institute of Technology (http://www-gpsg.mit.edu/~simon/gtgk). Figures were produced using the Generic Mapping Tools Software Package [*Wessel and Smith*, 1998]. We are particularly grateful to the GAMA network around the New Madrid Seismic Zone, maintained by the University of Memphis.

References

Altamimi, Z., X. Collilieux, and L. Métivier (2011), ITRF2008: An improved solution of the international terrestrial reference frame, *J. Geod.*, *85*, 457–473, doi:10.1007/s00190-011-0444-4.

Anderson, J. G. (1979), Estimating the seismicity from geological structure for seismic-risk studies, *Bull. Seismol. Soc. Am.*, *69*, 135–158.

Argus, D., and R. G. Gordon (1996), Tests of the rigid-plate hyopthesis and bounds on intraplate deformation using geodetic data from very long baseline interferometry, *J. Geophys. Res.*, *101*, 13,555–13,572.

Blewitt, G., and D. Lavallée (2002), Effect of annual signals on geodetic velocity, *J. Geophys. Res.*, *107*(B7), ETG 9-1–ETG 9-11, doi:10.1029/2001JB000570.

Bollinger, L., M. Nicolas, and S. Marin (2010), Hydrological triggering of the seismicity around a salt diapir in Castellane, France, *Earth Planet. Sci. Lett.*, *290*(1–2), 20–29.

Boyd, O., E. Calais, J. Langbein, H. Magistrale, S. Stein, and M. Zoback (2013), Workshop on new madrid geodesy and the challenges of understanding intraplate earthquakes, *U.S. Geol. Surv. Open File Rep., 2013-0031*, 184 pp., U.S. Geol. Surv., Reston, Va.

Calais, E., and S. Stein (2009), Time-variable deformation in the New Madrid Seismic Zone, *Science*, *323*, 1442, doi:10.1226/science.1168122.

Calais, E., G. Mattioli, C. DeMets, J. Nocquet, S. Stein, A. Newman, and P. Rydelek (2005), Tectonics strain in plate interiors?, *Nature*, *438*, E9–E10, doi:10.1038/nature04428.

Calais, E., J. Y. Han, C. DeMets, and J. M. Noquet (2006), Deformation of the North American plate interior from a decade of continuous GPS measurements, *J. Geophys. Res.*, *111*, B06402, doi:10.1029/2005JB004253.

Calais, E., A. M. Freed, R. Van Arsdale, and S. Stein (2010), Triggering of New Madrid seismicity by late-pleistocene erosion, *Nature*, *466*, 608–611, doi:10.1038/nature09258.

Cox, R. T., R. V. Arsdale, J. Harris, S. Forman, W. Beard, and J. Galluzzi (2000), Quaternary faulting in the southern Mississippi embayment and implications for tectonics and seismicity in an intraplate setting, *Geol. Soc. Am. Bull.*, *112*, 1724–1735.

Crone, A. J., and K. V. Luza (1990), Style and timing of Holocene surface faulting on the Meers fault, southwestern Oklahoma, *Geol. Soc. Am. Bull.*, *102*, 1–17.

Crone, A. J., P. M. De Martini, M. N. Machette, K. Okumura, and J. R. Prescott (2003), Paleoseismicity of two historically quiescent faults in Australia: Implications for fault behavior in stable continental regions, *Bull. Seismol. Soc. Am.*, *93*(5), 1913–1934.

Dixon, T. H., A. Mao, and S. Stein (1996), How rigid is the stable interior of the North American plate?, *Geophys. Res. Lett.*, *23*, 3035–3038.

Dunn, M., S. Horton, H. DeShon, and C. Powell (2010), High-resolution earthquake relocation in the New Madrid Seismic Zone, *Seismol. Res. Lett.*, *81*, 406–413, doi:10.1785/gssrl.81.2.406.

Frankel, A., R. Smalley, and J. Paul (2012), Significant motions between GPS Sites in the New Madrid region: Implications for seismic hazard, *Bull. Seismol. Soc. Am.*, *102*, 479–489, doi:10.1785/0120100219.

Fuller, M. L. (1912), *The New Madrid Earthquake*, vol. 494, U.S. Gov. Print. Off., Washington, D. C.

Galgana, G. A., and M. W. Hamburger (2010), Geodetic observations of active intraplate crustal deformation in the Wabash Valley Seismiz Zone and the Southern Illinois Basin, *Seismol. Res. Lett.*, *81*, 699–714, doi:10.1785/gssrl.81.5.699.

Gan, W., and W. H. Prescott (2001), Crustal deformation rates in central and eastern U.S. inferred from GPS, *Geophys. Res. Lett.*, *28*, 3733–3736.

Grollimund, B., and M. D. Zoback (2001), Did deglaciation trigger intraplate seismicity in the New Madrid Seismic Zone, *Geology*, *29*, 175–178.

Hamburger, M. W., V. Rybakov, A. Lowry, B. Shen-Tu, and J. A. Rupp (2002), Preliminary results from a GPS network in the Southern Illinois Basin, *Seismol. Res. Lett.*, *73*, 762–775.

Herring, T. (2003), MATLAB tools for viewing GPS velocities and time series, *GPS Solutions*, *7*, 194–199, doi:10.1007/s10291-003-0068-0.

Herring, T. A., R. W. King, and S. C. McClusky (2013), *Introduction to GAMIT–GLOBK Release 10.5*, Dep. of Earth Atmos. and Planet. Sci., Mass. Inst. of Technol., Cambridge.

Holbrook, J., W. J. Autin, T. M. Rittenour, S. Marshak, and R. J. Goble (2006), Stratigraphic evidence for millennial-scale temporal clustering of earthquakes on a continental-interior fault: Holocene Mississippi River floodplain deposits, New Madrid Seismic Zone, USA, *Tectonophysics*, *420*(3–4), 431–454.

Hough, S. E., and M. Page (2011), Toward a consistent model for strain accrual and release for the New Madrid Seismic Zone, central United States, *J. Geophys. Res.*, *116*, B03311, doi:10.1029/2010JB007783.

Hough, S. E., J. G. Armbruster, L. Seeber, and J. F. Hough (2000), On the modified Mercalli intensities and magnitudes of the 1811–1812 New Madrid earthquakes, *J. Geophy. Res.*, *105*(B10), 23,839–23,864.

Johnston, A. C. (1996), Seismic moment assessment of stable continental earthquakes—III. 1811–1812 New Madrid, 1886 Charleston, and 1755 Lisbon, *Geophys. J. Int.*, *126*, 314–344.

Kelson, K. I., G. D. Simpson, R. B. VanArsdale, C. C. Haraden, and W. R. Lettis (1996), Multiple late Holocene earthquakes along the reelfoot central New Madrid Seismic Zone, *J. Geophys. Res.*, *101*, 6151–6170.

Keranen, K. M., H. M. Savage, G. A. Abers, and E. S. Cochran (2013), Potentially induced earthquakes in Oklahoma, USA: Links between wastewater injection and the 2011 M_W 5.7 earthquake sequence, *Geology*, *41*, 699–702.

Kogan, M. G., G. M. Steblov, R. W. King, T. A. Herring, D. I. Frolov, S. G. Egorov, V. Y. Levin, A. Lerner-Lam, and A. Jones (2000), Geodetic contraints on the rigidity and relative motion of Eurasia and North America, *Geophys. Res. Lett.*, *27*, 2041–2044.

Langbein, J. (2004), Noise in two-color electronic distance meter measurements revisited, *J. Geophys. Res.*, *109*, B04406, doi:10.1029/2003JB002819.

Liu, L., M. D. Zoback, and P. Segall (1992), Rapid intraplate strain accumulation in the New Madrid seismic zone, *Science*, *257*, 1666–1669.

McBride, J. H., T. G. Hildenbrand, W. J. Stephenson, and C. J. Potter (2002), Intepreting the earthquake source of the Wabash Valley seismic zone (Illinois, Indiana, and Kentucky) from seismic-reflection, gravity, and magnetic-intensity data, *Seismol. Res. Lett.*, *73*, 660–686.

Newman, A., S. Stein, J. Weber, J. Engeln, A. Mao, and T. Dixon (1999), Slow deformation and lower seismic hazard at the New Madrid Seismic Zone, *Science*, *284*, 619–621.

Nocquet, J. M., E. Calais, and B. Parsons (2005), Geodetic constraints on glacial isostatic adjustment in Europe, *Geophys. Res. Lett.*, *32*, L06308, doi:10.1029/2004GL022174.

Nuttli, O. W. (1973), The Mississipi Velley earthquakes of 1811–1812: Intensities, ground motion and magntiudes, *Bull. Seismol. Soc. Am.*, *63*, 227–248.

Nuttli, O. W., and K. G. Brill (1981), Earthquake source zones in the central United States determined from historical seismicity, in *Approach to Seismic Zonation for Siting Nuclear Electric Power Generating Facilities in the Eastern United States, U. S. Nucl. Regul. Comm. Rep. NUREG/CR-1577*, edited by R. Barstow et al., pp. 98–143, U.S. Nucl. Regul. Comm., Springfield, Va.

Obermeier, S. F. (1998), Liquifaction evidence for strong earthquake of Holocene and latest Pleistocene ages in the states of Indiana and Illinois, USA, *Eng. Geol.*, *50*, 227–254.

Page, M. T., and S. E. Hough (2014), The New Madrid Seismic Zone: Not dead yet, *Science*, *343*, 762–764, doi:10.1126/science.1248215.

Petit, G., and B. Luzum (2010), IERS conventions (2010), *Tech. Rep. DTIC Document*, Verlag des Bundesamts für Kartographie und Geodäsie, Frankfurt am Main, Germany.

Potter, C. J., M. B. Goldhaber, and P. C. Heigold (1995), *Structure of the Reelfoot-Rough Creek Rift System, Fluorspar Area Fault Complex, and Hicks Dome, Southern Illinois and Western Kentucky-New Constraints From Regional Seismic Reflection Data, U.S. Geol. Surv. Prof. Pap. 1539-Q*, U.S. Gov. Print. Off., Washington, D. C.

Reilinger, R., et al. (2006), GPS constraints on continental deformation in the Africa-Arabia-Eurasia continental collision zone and implications for the dynamics of plate interactions, *J. Geophys. Res.*, *111*, B05411, doi:10.1029/2005JB004051.

Schmid, R., P. Steigenberger, G. Gendt, M. Ge, and M. Rothacher (2007), Generation of a consistent absolute phase centre correction model for GPS receiver and satellite antennas, *J. Geod.*, *81*, 781–798, doi:10.1007/s00190-007-0148-y.

Sella, G. F., S. Stein, T. H. Dixon, M. Craymer, T. S. James, S. Mazzotti, and R. K. Dokka (2007), Observation of glacial isostatic adjustment in "stable" North America with GPS, *Geophys. Res. Lett.*, *34*, L02306, doi:10.1029/2006GL027081.

Smalley, R., M. A. Ellis, J. Paul, and R. B. Van Arsdale (2005), Space geodetic evidence for rapid strain rates in the New Madrid Seismic Zone of central USA, *Nature*, *435*, 1088–1090, doi:10.1038/nature03642.

Snay, R. A., J. F. Ni, and H. C. Neugebauer (1994), *Geodetically Derived Strain Across the Northern New Madrid Seismic Zone, U.S. Geol. Surv. Prof. Pap. 1538-F2*, U.S. Gov. Print. Off., Washington, D. C.

Stein, S., and M. Liu (2009), Long aftershock sequences within continents and implications for earthquake hazard assessment, *Nature*, *462*, 87–89, doi:10.1038/nature08502.

Tuttle, M. P., E. S. Schweig, J. D. Sims, R. H. Lafferty, L. W. Wolf, and M. L. Haynes (2002), The earthquake potential of the New Madrid Seismic Zone, *Bull. Seismol. Soc. Am.*, *92*, 2080–2089.

Tuttle, M. P., E. S. Schwieg III, J. Campbell, P. N. Thomas, J. D. Sims, and R. H. Lafferty III (2005), Evidence for New Madrid earthquakes in A.D. 300 and 2350 B.C., *Seismol. Res. Lett.*, *76*, 489–502.

Van Arsdale, R. B. (2009), *Adventures Through Deep Time: The Central Mississippi River Valley and Its Earthquakes, Geol. Soc. Am. Spec. Pap. 455*, Geol. Soc. Am., Boulder, Colo.

Wessel, P., and W. Smith (1998), New, improved version of generic mapping tools released, *Eos Trans. AGU*, *79*(47), 579–579.

Wheeler, R. L., and A. J. Crone (2001), Known and suggested Quaternary faulting in the mid-continent United States, *Eng. Geol.*, *62*, 51–78.

Williams, S. D. P. (2003), The effect of coloured noise on the uncertainties of rates estimated from gedoetic time series, *J. Geod.*, *76*, 483–494, doi:10.1007/s00190-002-0283-4.

Williams, S. D. P. (2008), CATS: GPS coordinate time series analysis software, *GPS Solutions*, *12*, 147–153, doi:10.1007/s10291-007-0086-4.

Wu, P., and P. Johnston (2000), Can deglaciation trigger earthquakes in N. America?, *Geophys. Res. Lett.*, *27*, 1323–1326.